

# Taking into account the swelling and shrinkage of expansive soils in the design and behavior of pavements

## 1. INTRODUCTION

The development of road infrastructure is crucial for a nation's socio-economic vitality. Well-designed roads facilitate easy and immediate access to essential services, the transport of goods and people, stimulate socio-economic development, and strengthen regional and national connectivity. As one of the socio-economic lifelines of any country, it is paramount to guarantee the stability, durability, and meticulous monitoring of roads throughout their lifespan. To achieve this, it is necessary to carefully plan and examine the road structure, which consists of several layers that support traffic, ensure stability, comfort, and efficient rainwater drainage, resist deformation and settlement caused by traffic and climatic variations, and facilitate reliable maintenance and repair to extend the structure's durability and service life. Pavements, as geotechnical structures, are built on natural soils known as subgrade. These subgrades, acting as road subgrades, must be rigorously studied to ensure their capacity to support all road loads and guarantee the overall health of the road. This often-overlooked connection plays a crucial role in the long-term stability and performance of roads, particularly when the pavement is built on clay soils that are sensitive to climatic variations, causing significant volumetric changes. Water added to clay soils causes them to expand (swell), while water loss leads to contraction (shrinkage), thus influencing the geotechnical behavior of the soil. This phenomenon of variation in the water content of clay soils (swelling-shrinkage phenomenon) causes premature failures in pavements. This phenomenon is observed on a section of National Inter-State Route 2 (RNIE 2) in Benin, the main road linking the south to the north of Benin, crossing a depression known as the Lama Depression in the south of the country, between the Atlantique department, Toffo commune, Sèhouè district, and the Zou department, Zogbodomey commune, Massi district. This region is characterized by a high concentration of swelling soils, particularly swelling clay, found to a depth of up to 30 meters. Several factors, such as mineralogical and organic composition, water content, climatic conditions, and particle size distribution, underlie the swelling-shrinking cycle of clay and strongly influence the geotechnical properties of clay soils, thus impacting the behavior of expansive soils. Finding solutions to this phenomenon remains a matter of in-depth consideration, as it is impossible to circumvent these soils in some areas. However, it should be noted that research projects have been carried out by researchers to further understand the parameters characterizing swelling clays in the Lama Depression. The study of the shear and compressibility behavior of expansive soils subjected to shrink-swell cycles under pavements: the case of the Sèhouè-Massi section over eight cycles shows that it is a very plastic and inorganic clay ( $I_p = 45$ ,  $MO = 0.7\%$ ), shows a decrease in cohesion to 42.98 kPa and in the friction angle to  $14.6^\circ$  with an increase in the compressibility index and a decrease in the swelling index, highlighting the importance of managing these variations to maintain pavement stability

38 and minimize the adverse effects of shrink-swell cycles on road infrastructure. [1] . A study  
39 on the behavior of swelling soils in the Lama depression and its interaction with shallow  
40 foundations: the case of the Kho depression made it possible to observe the reduction of  
41 the swelling potential of these soils under the effect of the saline solution, to include a  
42 modeling of the interaction of these soils with shallow foundations and to propose design  
43 recommendations to minimize the settlement of structures built on these soils [2] .  
44 Evaluation of the influence of drying-wetting cycles on the compressibility of clay soils in the  
45 commune of HouéyogbéThe study in the Lama depression shows that the soil is class A3  
46 clay, subjected to drying-wetting cycles with an increase in compressibility index, a  
47 decrease in swelling index, stability of pre-consolidation pressure and oedometer modulus,  
48 and a notable increase in soil permeability with the number of cycles [3] . The impact of  
49 swelling on the settlement of clay soils in the municipality of Houeyogbe in the Lama  
50 depression shows that these are plastic clays with free swelling, which partially influences  
51 the final settlement value [4] . The behavior of shallow foundations evaluated on swelling  
52 soils in the Issaba and Ahoyéyé areas of the municipality of Pobè, by comparing the results  
53 of the Plaxis and Géofond software , highlighted the differences in bearing capacities [5] .  
54 The macroscopic and microscopic study of clay soils in the regions ( Adjaïgbonou , Kpinnou  
55 , Ouèdèmè and Lokossa) shows the limitations of existing geotechnical characterization  
56 methods for determining the swelling potential of clay soils using indirect methods based on  
57 parameters such as particle size, Atterberg limits and methylene blue value [6] .  
58 A physico-mechanical characterization of clay soils in the Issaba depression in southeastern  
59 Benin revealed that they are highly plastic clay particles with a high swelling potential and a  
60 high risk of pathology [7] . Stabilization of swelling soils in the Oran region using saline  
61 solutions, sand addition, and stabilization with lime, cement, or lime-cement resulted in a  
62 reduction of up to 80% in swelling [8] . An examination of the swelling and shrinkage  
63 potential of clay soils under road surfaces in the marshlands of southwestern France  
64 revealed a high clay content and a certain sensitivity to swelling and shrinkage [9] . The  
65 characterization and estimation of swelling in Algerian clays, specifically the clays of Médéa,  
66 has shown a correlation between the empirical methods applied and the evolution of the  
67 clay structure during shrinkage-swelling. This is being monitored with the aim of  
68 understanding the swelling mechanism [10] . The effect of lime content on the bearing  
69 capacity and swelling potential of an expansive soil, through stabilization tests at 0%, 2%,  
70 4%, 6%, 8%, and 10% lime, resulted in an improvement in the bearing capacity and a  
71 decrease in the swelling potential of the expansive soil with the addition of lime [11] .  
72 Prediction of California rolling rate of expansive soils using Gaussian process regression by  
73 hydrated lime-activated rice hull ash (HARHA) of treated soil input data: hybrid geometric  
74 binder, liquid limit, plasticity limit, plasticity index, optimum moisture content and maximum  
75 dry density, affirmed that HARHA was the key sensitive parameter affecting the CBR of  
76 expansive soils [12] . The jute fiber test on the CBR value of expansive soil demonstrated  
77 that adding 10 mm and 30 mm jute fibers at various percentages (0.25%, 0.50%, 0.75%,

78 1%, 1.25%, and 1.50% of the soil dry weight) significantly improves the CBR value of the  
79 expansive soil, with a maximum increase of 226.92% for an optimal jute fiber content of  
80 1.25%. This suggests an economical solution for strengthening clay soils with agricultural  
81 waste [13] . An experimental study of the geotechnical properties and microstructure of  
82 expansive soils stabilized with granite dust showed that adding up to 20% granite dust  
83 significantly improves the unconfined compression and CBR of expansive soils. Further  
84 research was conducted to optimize the stabilization of these soils.

85 With this in mind, the present work aims to contribute to the understanding of the swelling-  
86 shrinking phenomenon of expansive soils in order to create a parametric connection  
87 between pavement design and the characterization of clay soils under the stresses of  
88 swelling-shrinking cycles to anticipate their movement under pavements in the long term by  
89 exploring eight cycles to ensure the stability and durability of pavements.

## 90 2. METHOD

### 91 2.1. Study area and sampling

92 Clay samples were collected from the Lama depression near National Interstate Route No. 2  
93 ( RNIE No. 2 ) in Benin, on the Akassato -Bohicon section between Sèhouè and Massi. The  
94 geographical coordinates of the sampling point are shown in Table 1:

95 *Table 1: Geographic coordinates of the sample*

<i>Contact details</i>			
X	Y	Latitude	Longitude
59454217	22630897	N:	E:
		767774.54m	418566.822m

### 96 2.2. Sampling techniques

97 To carry out the physico-mechanical tests encompassing both identification and mechanical  
98 tests, a mixture of samples taken from the following depths: 0 to 0.50 m; 0.5 to 1.0 m; 1.0  
99 to 1.50 m; 1.50 to 2 m and 2 m to 2.50 m were obtained.

### 100 2.3. Description of the tests

- 101 ○ Identification tests:
- 102 - Determination of water content NF EN ISO 17892-1
  - 103 - Particle size analysis by sieving and sedimentation (NF EN ISO 17892-4)
  - 104 - Atterberg limit tests NF EN ISO 17892-12
  - 105 - Methylene blue value test NF EN 933-9
  - 106 - Specific weight EN ISO 17892-3
  - 107 - Organic matter content NF P 94 – 055

108 ○ Mechanical tests

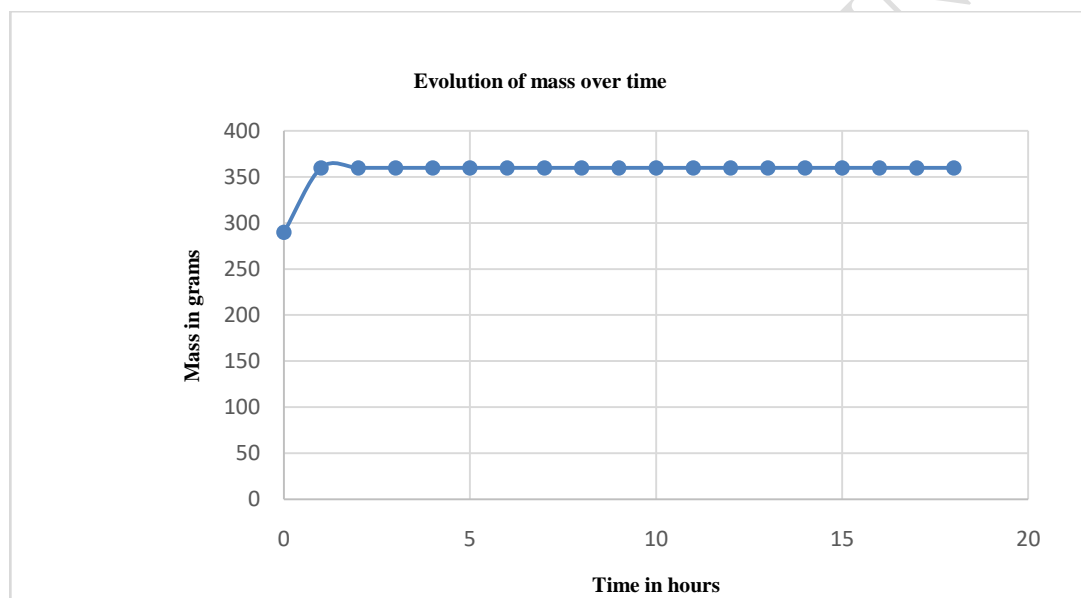
109 - Modified Proctor test NF P94-093.

110 - The samples of disturbed soil that had undergone wetting-drying cycles were subjected to  
111 the CBR NF P 94-078 test.

#### 112 **2.4.Operating procedure for the humidification and drying cycle**

113 a) Clay samples were placed in Dangote bags and immersed in water. After 24 hours,  
114 they were weighed hourly until their mass stabilized, indicating complete water saturation.  
115 Simultaneously, control samples were dried in an oven and in the sun to measure the water  
116 content after wetting and natural drying.

117



118

119

*Figure 1: Humidification kinetics*

120 b) The clay samples are dried in the sun at temperatures ranging from 24°C to 48°C  
121 for 9 hours a day, simulating the shrinkage phenomenon during the dry season. This allows  
122 them to reach a drying moisture content of 14%, similar to that measured in the swelling  
123 clays of the Lama depression.

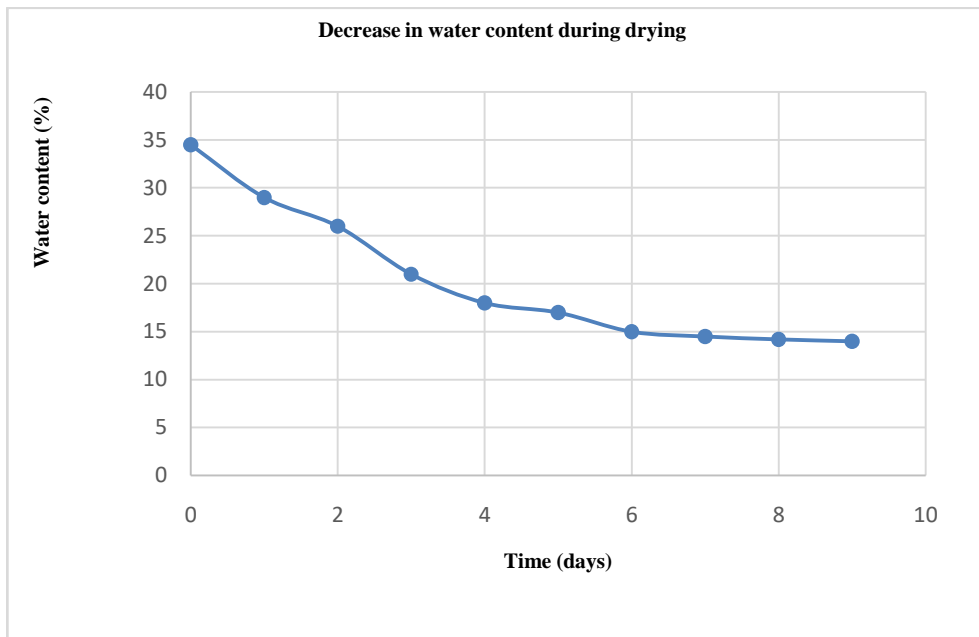


Figure 2: Drying kinetics

124

125

126 c) Description and interpretation of sample textures during cycles

127 When wet, clay absorbs water, causing it to expand and increase in volume. As it dries, the  
 128 evaporated water causes the clay to contract, leading to cracks on its surface. With each  
 129 cycle of wetting and drying, the clay becomes more susceptible to volume changes,  
 130 resulting in a weakening of its structure. This material fatigue is due to the progressive  
 131 breaking of bonds between clay particles, resulting in a more cracked and brittle texture as  
 132 the cycle repeats.



133

134 *Photo 1: Illustration of the texture of samples that have undergone humidification-drying*  
135 *cycles*

136 After each drying cycle, the material is ground in a metal mold and sieved through a 5 mm  
137 sieve. The sieve passages are then used to determine the moisture content of the ground  
138 material, in order to perform the CBR test.

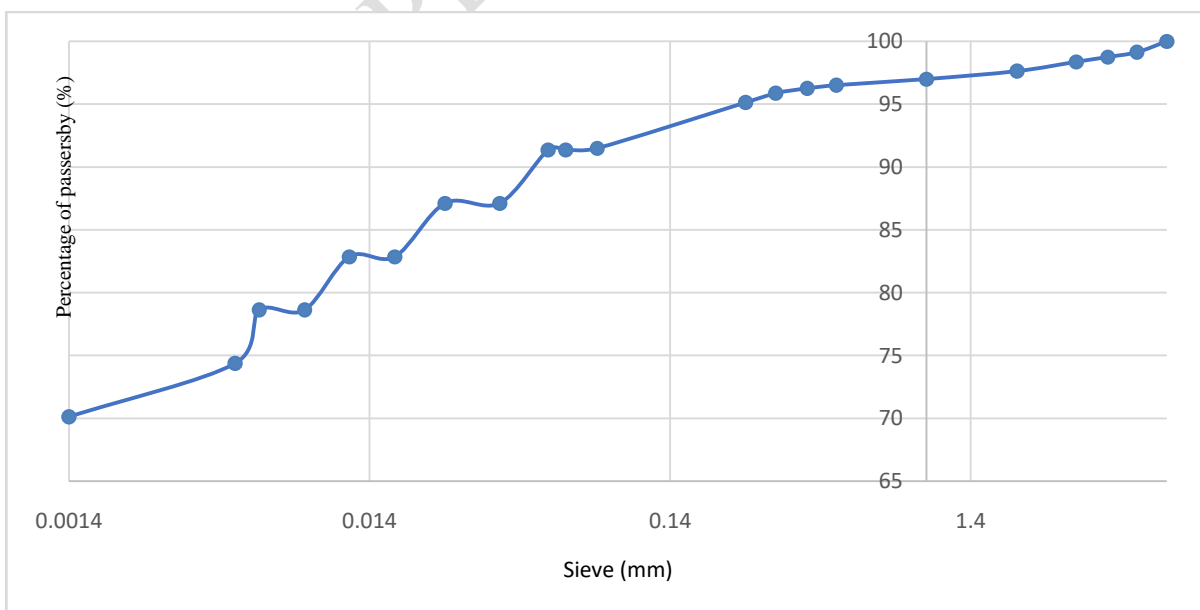


139  
140 Photo 2: Preparing the sample to be used

### 141 3. RESULTS

#### 142 3.1. Identification tests

143 Figure 4 shows the particle size distribution of the soil studied. The percentage passing  
144 through the 80  $\mu\text{m}$  sieve is 91.50%, which is greater than 35%, therefore the soil studied is  
145 a fine soil.



146

147

148

Figure 3: Particle size distribution curve of the clay from the Lama depression (Sèhouè-Massi section )

149

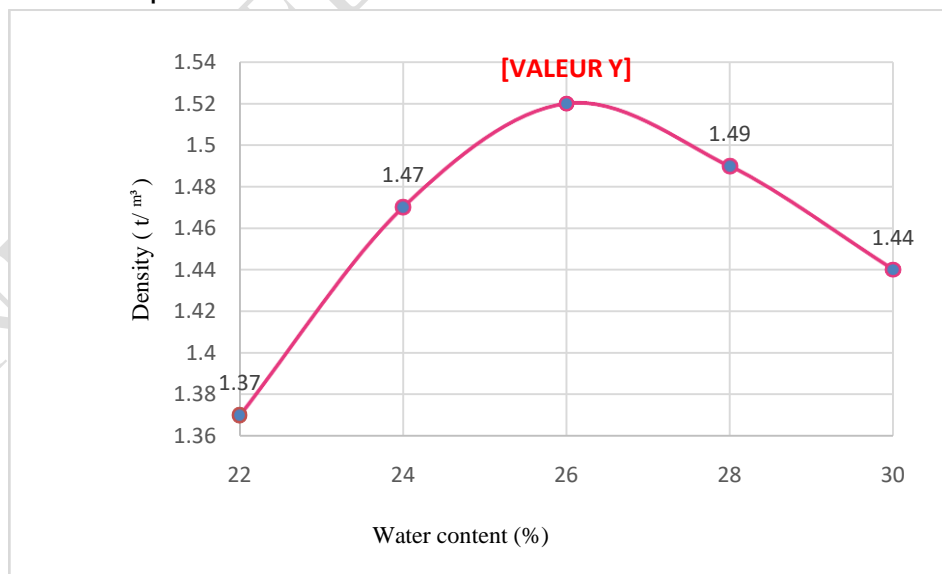
150

Table 2: Summary of identification tests

Parameters Values	
Natural water content $w$ (%)	35.85
Passage through 80 $\mu$ m (%)	91.50
Passing through a 2 $\mu$ m sieve $C_2$ (%)	71
Methylene blue value VBS	13,714
Liquidity limit $w_L$ (%)	33.3
Plastic limit $w_P$ (%)	47
Plasticity Index $I_P$ (%)	36.3
Consistency Index $I_C$	1.31
Organic matter OM (%)	0.65
Specific weight $\gamma_s$ (g.cm <sup>-3</sup> )	2,101
Blue activity of the clay fraction $A_{CB}$	19.315 > 18

151 **3.2. Mechanical tests**

152 Figure 5 shows the Proctor curve of the soil studied. The maximum dry density is 1.52  
153 t/m<sup>3</sup>, obtained at an optimal content of 27.5%.

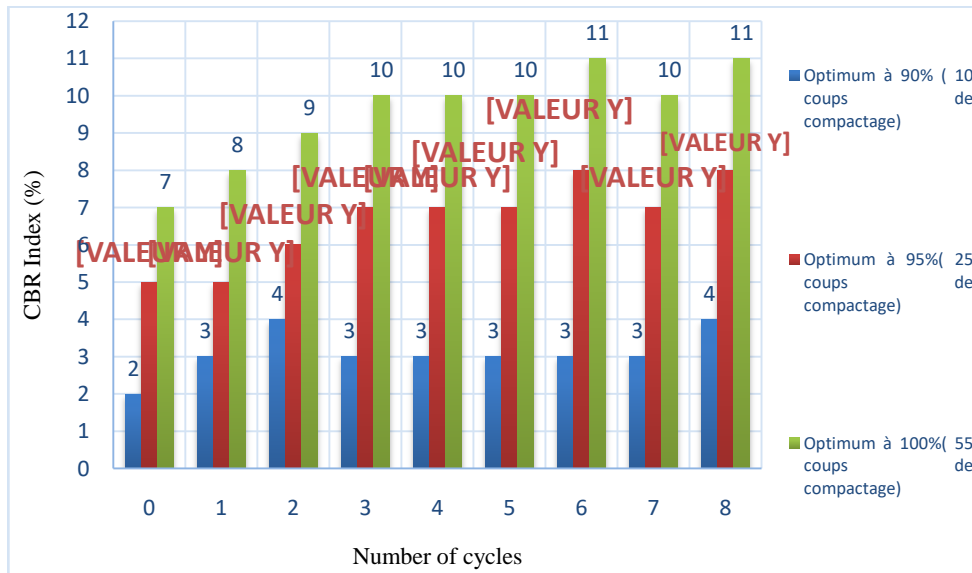


154

Figure 4: Modified Proctor curve of the studied clay

155

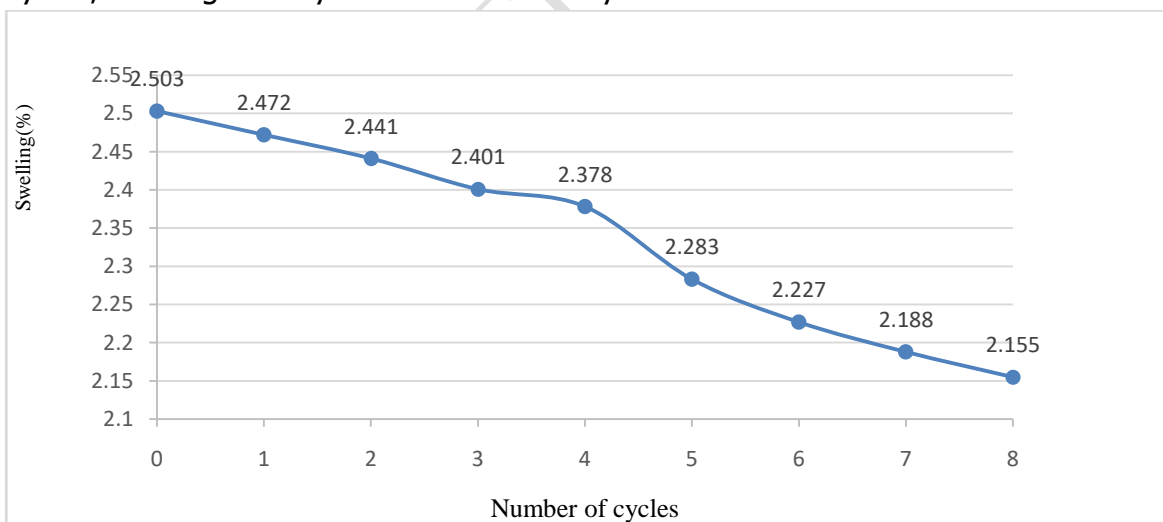
156 To assess the influence of swelling-shrinkage cycles on the bearing capacity of the clay  
 157 studied, the CBR indices of the samples were determined over eight wetting-drying cycles.  
 158 Figure 6 shows the variation of the CBR index as a function of the number of wetting-drying  
 159 cycles, where the CBR index, taken at 95%, increases by approximately 60% with the  
 160 number of cycles.



161

162 *Figure 5: Variation of the soil CBR index as a function of the wetting-drying cycle*

163 Figure 8 illustrates the evolution of CBR mold swelling as a function of wetting-drying  
 164 cycles, which gradually decreases as the cycle increases.



165

166 *Figure 6: Evolution of swelling in the CBR mold as a function of wetting-drying cycles*

### 167 **2.5.Pavement structure design (Sèhouè- Massi section)**

168 The pavement design for the Sèhouè-Massi section of National Highway 2 (RNIE 2),  
 169 crossing the Lama depression, was carried out using the Algerian catalog for the design of

170 new pavements (CTTP 2001) ,adapted to the CBR index and extreme design parameters.  
 171 The 7-meter-wide, two-way pavement extends from the southern access road to Séhouè  
 172 (km 78+456) to the northern exit of Massi (km 86+720), with an estimated traffic volume  
 173 of 820 heavy goods vehicles per day in each direction in 2026, corresponding to a reference  
 174 load of 13 tonnes (traffic class TPL5). The method used for classifying the studied soil is  
 175 based on an empirical formula where the Young's modulus E (in MPa) is equal to five times  
 176 the soil's CBR bearing capacity index .The values obtained remain low, and the soil has  
 177 been classified as S3, requiring upgrading to S1 to guarantee the stability of the structure.  
 178 The area is classified as climate zone III , with a projected service life of 15 years and a  
 179 geometric growth of 3%. The pavement structure selected according to catalog booklet 3  
 180 comprises: 6 cm of bituminous concrete (BB) as a surface course, 12 cm of bituminous  
 181 gravel (GB) as a base course, 35 cm of untreated gravel (GNT) as a subbase, and 70 cm of  
 182 lateritic gravel (GL) distributed in two subgrade layers. This design has been optimized to  
 183 address the problems caused by soil swelling and shrinkage phenomena in order to  
 184 guarantee the stability and durability of the pavement under seasonal variations.

185 *Table 3: Properties of pavement and subgrade materials according to the cycle*

Pavement layers	Materials	Layer thicknesses (m)	Young's modulus (MPa)	Poisson's ratio ( $\nu$ )
Wearing course	Bituminous concrete (BB)	0.06	3500	0.35
Base layer	Bituminous gravel (GB)	0.12	5500	0.35
Foundation layer	Severe untreated (GNT)	0.35	350	0.25
Form layer	Gravelly lateritic GL	0.35	280	0.25
	Gravelly lateritic GL	0.35	280	0.25
Swelling clay soil	Cycle 0	Infinity	25	0.35
	Cycle 1	Infinity	25	0.35
	Cycle 2	Infinity	30	0.35
	Cycle 3	Infinity	35	0.35
	Cycle 4	Infinity	35	0.35
	Cycle 5	Infinity	35	0.35
	Cycle 6	Infinity	40	0.35
	Cycle 7	Infinity	35	0.35
	Cycle 8	Infinity	40	0.35

186 The base layer is made of bitumen-treated materials, so we check if  $\varepsilon_t$  and  $\varepsilon_z$ , calculated  
 187 using Alize III, are below the permissible values.

188 *Table 4: Summary of deformations at the base of the bituminous gravel and in the subgrade*  
 189 *according to the cycle*

Number of cycles	Calculated vertical deformation $\varepsilon_z (10^{-6})$	Allowable vertical deformation $\varepsilon_{z,adm} (10^{-6})$	Tensile deformation at the base of GB $\varepsilon_t (10^{-6})$	Allowable tensile deformation $\varepsilon_{t,adm} (10^{-6})$
0	183.1	660.84	114.8	128,292
1	183.1		114.8	
2	171.5		114.8	
3	161.8		114.9	
4	161.8		114.9	
5	161.8		114.9	
6	153.4		114.9	
7	161.8		114.9	
8	153.4		114.9	

190 The vertical strain  $\varepsilon_z$  decreases by about 16.2% while the tensile strain  $\varepsilon_t$  increases slightly  
 191 by 0.09%, but in both cases they remain below the allowable values  $\varepsilon_{z,adm}$  and  $\varepsilon_{t,adm}$ ,  
 192 verifying the design conditions in each case.

193 
$$\varepsilon_t < \varepsilon_{t,adm} ; \varepsilon_z < \varepsilon_{z,adm}$$

194 **2.6. Numerical modeling and simulation of the pavement using the ABAQUS finite**  
 195 **element software**

196 The pavement, designed for expansive clay soil, was modeled using ABAQUS 2021  
 197 software, taking into account the swelling and shrinkage cycles.

198 - **Model geometry and characteristics of the supporting soil**

*Tableau 5: Propriétés de cisaillement du sol étudié*

Number of cycles	Young's modulus E (MPa)	Poisson's ratio ( $\nu$ )	Angle of friction $\varphi_u$ (°)	Cohesion $C_u$ (Kpa)	Unsaturation density (kg/m <sup>3</sup> )	density (kg/m <sup>3</sup> )
0	25	0.35	14.6	42.98	1465.85	1800.2
1	25	0.35	6.9	16.81	1695.21	2264.02

2	30	0.35	5.5	15.89	1307.85	2360.86
3	35	0.35	5.2	14.72	1320.08	2545.36
4	35	0.35	5.1	14.21	1357.8	2628.95
5	35	0.35	5.05	13.50	1147.81	2300.71
6	40	0.35	5	13.30	1314.98	2545.36
7	35	0.35	4.8	12.9	1357.8	2628.95
8	40	0.35	4.71	11.47	1357.8	2628.95

199 Shear properties are used in the Mohr-Colomb model under ABAQUS to simulate the  
 200 behavior of expansive soils subjected to shrink-swell cycles, with a 3D geometric model of  
 201 dimensions 10x10x10m.

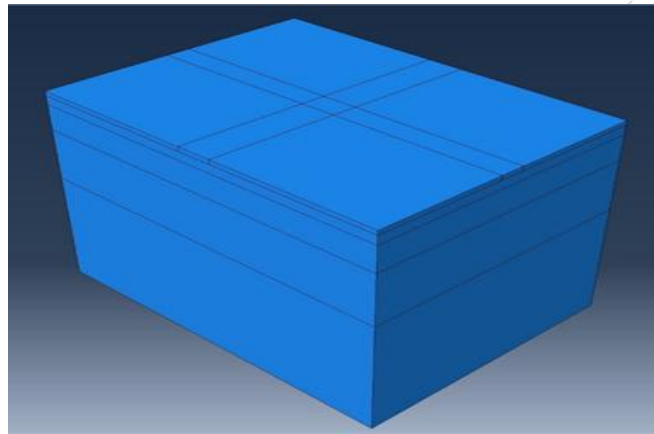


Figure 8: Géométrie du modèle

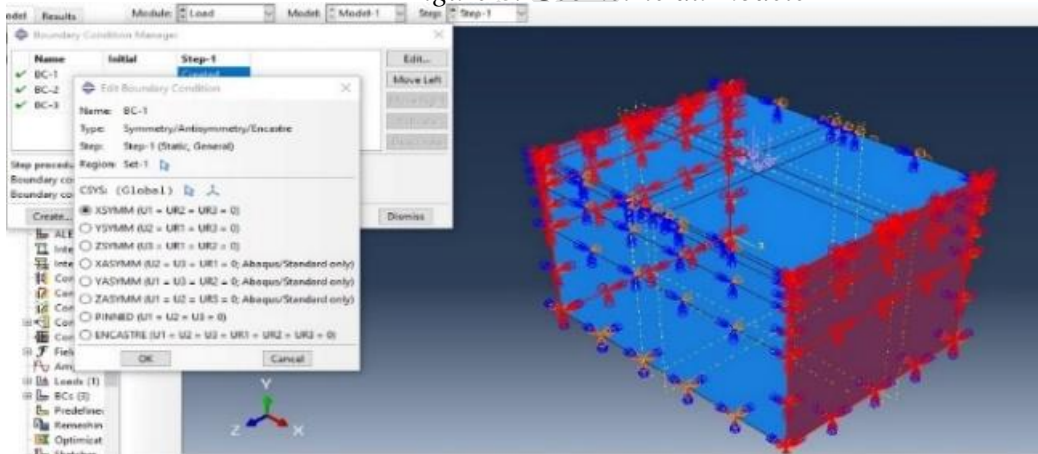


Figure 9: Contions aux limites du modèle

204 The traffic load applied to the pavement, modeled as a circle in ALIZE, is converted into a  
 205 rectangular load 0.38 m long and 0.26 m wide for use in ABAQUS, with a force of 65 kN  
 206 and a pressure of 0.329 MPa. The model was discretized with CAX4R elements in ABAQUS,  
 207 using finer elements near the loading area and coarser elements elsewhere, and a  
 208 parametric study assessed the impact of the number of elements on the convergence of the  
 209 results.

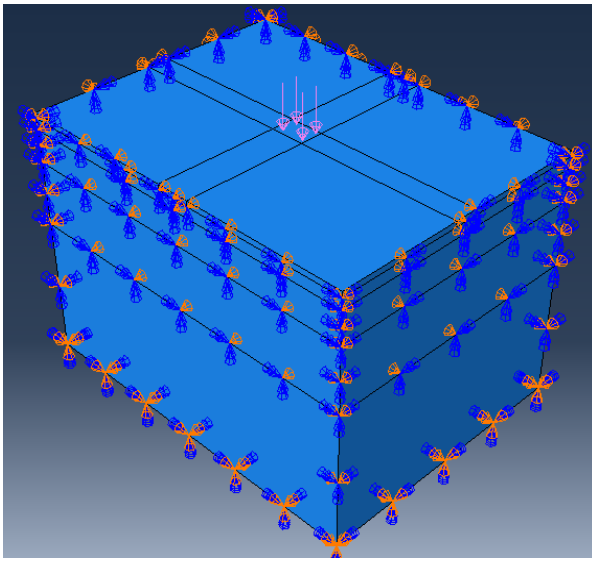


Figure 10 : Application de la charge surfacique

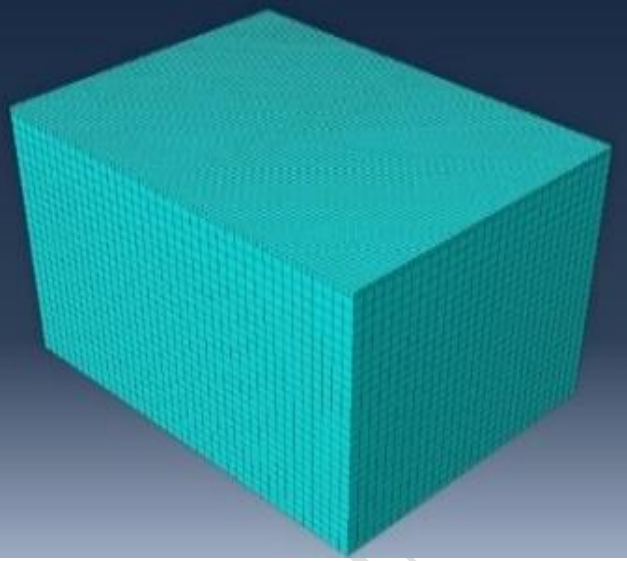


Figure 11 : Maillage

210

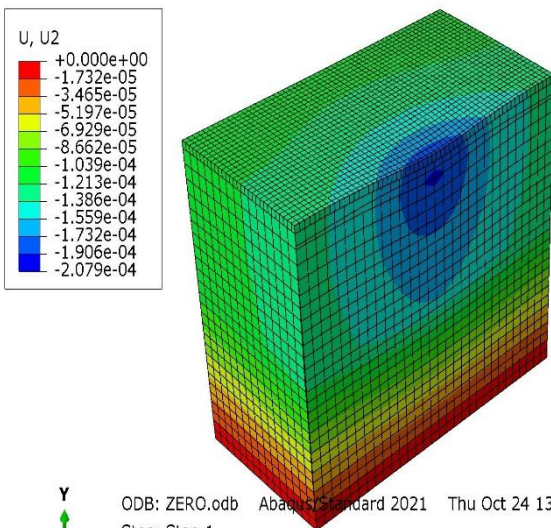
211

212 ○ Simulation results

213

214

215

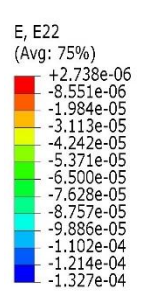


ODB: ZERO.odb Abaqus/Standard 2021 Thu Oct 24 13:00:39  
 Step: Step-1  
 Increment 1: Step Time = 1.000  
 Primary Var: U, U2  
 Deformed Var: U Deformation Scale Factor: 1.308e+03

216

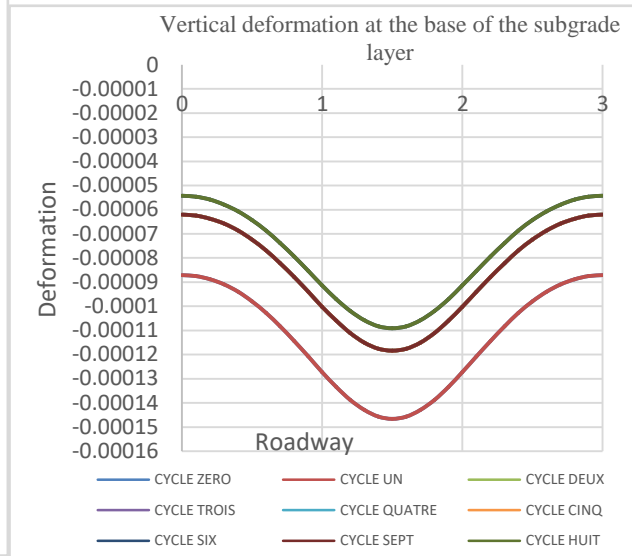
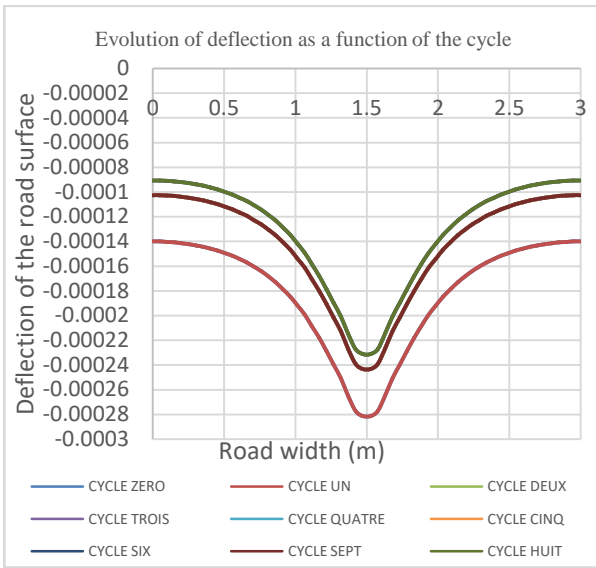
Figure 12: Champ de déflexions à la surface de la chaussée (cycle 0)

217



ODB: ZERO.odb Abaqus/Standard 2021 Thu Oct 24 13:00:39 Afr. centrale  
 Step: Step-1  
 Increment 1: Step Time = 1.000  
 Primary Var: E, E2  
 Deformed Var: U Deformation Scale Factor: 1.308e+03

Figure 13 : Champ de déformations à la base de la couche de forme ( cycle 0)

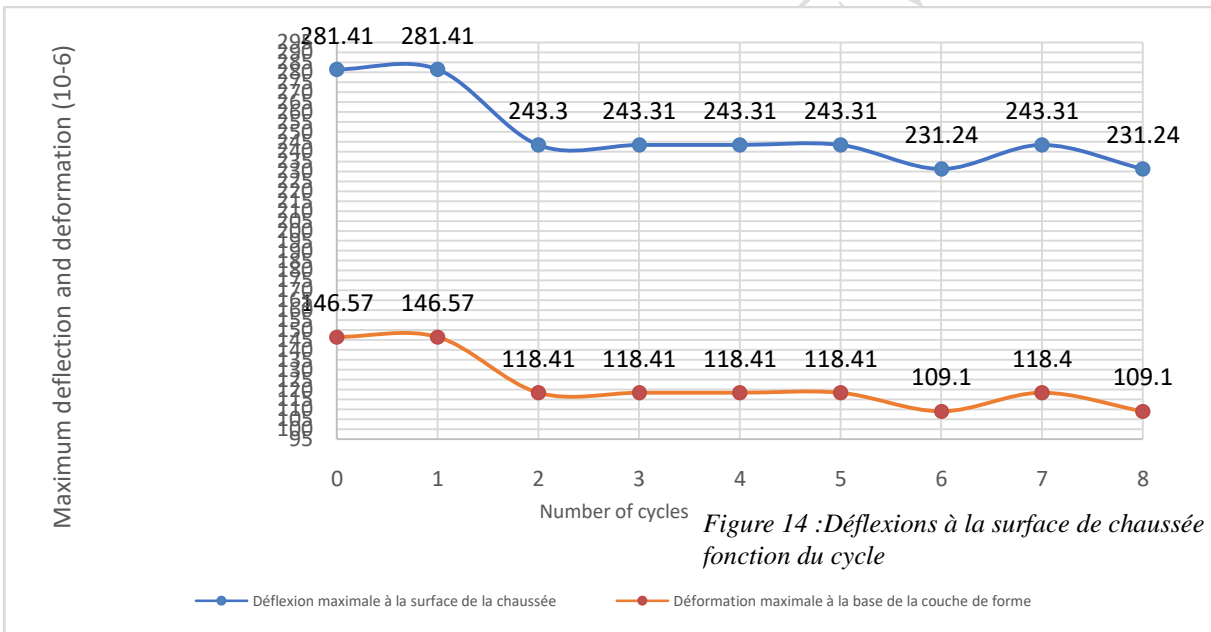


218

Figure 14 : Déflexions à la surface de chaussée en fonction du cycle

219

Figure 15 : Déformations verticales à la base de la couche de forme en fonction du cycle



220

Figure 16 : Déflexions à la surface de chaussée en fonction du cycle

221

Figure 16: Evolution des déflexions maximales à la surface de la chaussée et des déformations verticales maximales à la base de la couche de forme en fonction du cycle

222

The overall results reveal that the deflection at the surface of the pavement and the deformation at the base of the subgrade decrease by 17.82% and 25.56% respectively as the cycles progress.

224

225

### 3. DISCUSSION

226 Test results show that the soil studied is a swelling clay, very consistent and inorganic, with  
227 a high susceptibility to shrinkage and swelling. The maximum dry density is  $1.52 \text{ t/m}^3$ ,  
228 obtained at an optimal water content of 27.5%. The CBR index, measured at 95% of  
229 optimum, indicates an improvement in bearing capacity of approximately 60%, increasing  
230 from 5% to 8% after eight wetting-drying cycles, with swelling gradually decreasing and  
231 providing better stability. These cycles promote particle reorganization, reducing plasticity  
232 and limiting deformations due to moisture variations. The pavement design, carried out  
233 taking into account seasonal cycles according to the CTPP 2001 method, allows for the  
234 selection of materials ensuring good durability, stability, drainage, resistance to climatic  
235 variations, and a reduction in the risk of cracking. Simulation results show that the  
236 proposed multi-layer design improves pavement performance by reducing deflections and  
237 deformations. The soil will benefit from improved stability thanks to the management of  
238 water conditions, thus increasing its load-bearing capacity. To guarantee the longevity of  
239 the infrastructure, regular monitoring and maintenance, with targeted interventions,  
240 ensures a reliable and durable pavement that can withstand climatic hazards and load  
241 variations.

#### 242 **4. CONCLUSION**

243 Some roads in Benin cross the Lama Depression, a swelling clay zone, notably the National  
244 Interstate Route No. 2 linking the South and the North. This study, entitled "Consideration  
245 of Swelling-Shrinking of Expansive Soils in the Design and Behavior of Pavements,"  
246 examines the impact of swelling and shrinking cycles on the bearing capacity of clay soils  
247 and its consideration in pavement design. The results show that these cycles improve the  
248 soil's mechanical resistance, thus promoting pavement stability and durability. Numerical  
249 simulations in ABAQUS demonstrate that increasing the frequency of cycles reduces  
250 deflections and deformations, thereby enhancing the stability and longevity of the road  
251 infrastructure.

252 The results of this study led us to formulate the following recommendations to improve  
253 pavement performance:

- 254 - To implement real-time monitoring systems for soil conditions and pavement performance  
255 in order to anticipate failures;
- 256 - To explore innovative soil stabilization techniques such as the use of geopolymers and  
257 economical chemical treatments to strengthen the clay structure while respecting the  
258 environment;
- 259 - Encourage in-depth scientific research on the long-term behavior of swelling clay.

260 -

#### 261 **5. BIBLIOGRAPHICAL REFERENCES**

262 SOUNOUVOU Léonard , "shear and compressibility behavior of expansive soils subjected to  
263 shrink-swell cycles under pavements: case of the Sèhouè-Massi section ," *Angew. Chemie*  
264 *Int. Ed. 6(11), 951–952. , vol. 1, no. April, pp. 2022–2023.*

265 MEDETO Domaya Dominique , "Theme Study of the behavior of swelling soils in the Lama  
266 depression and its interaction with shallow foundations: case of the Kho depression ", 2021.  
267 I. Journal, E. Sciences, and IC Editor, "Influence of Drying-Wetting Cycles on the  
268 Compressibility of Clay Soils in the Commune of Houeyogbe," *Int. J.Eng. Sci. Res. Technol. ,*  
269 *flight. 10, no. 5, pp. 1–12, 2021, doi: 10.29121/ijesrt.v10.i5.2021.1.*

270 Z. Virtus, Influence of swelling on the population of clay soils in the Houeyogbe commune  
271 in the Lama depression, 2009

272 h. Donald, exploratory study of the behavior of shallow foundations on swelling soils: CASE  
273 OF ISSABA Presented, 2020 .

274 YST Kiki, "Mineralogical, thermal and microscopic characterization of fine soils in road  
275 construction," University of Bordeaux and University of Abomey-Calavi, France and Benin,  
276 2016 .

277 KJ Agbelele, G. Léopold, G. Aïsse, and AP Kla, "Physico-mechanical characterization of clay  
278 soils in the Issaba depression in Southeast Benin Summary," vol. 12, no. 2, pp. 206–221,  
279 2016.

280 A. Hachichi, SA Bourokba, and A. Benaïssa, "Study of shrinkage-swelling and stabilization  
281 phenomena of expansive soils in the Oran region Abstract: Abstract:," no. January, 2009.

282 MA Es-soufi, J. Saliba, and N. Saiyouri, "Study of the swelling and shrinkage potential of  
283 clay soils under the road surface of marsh roads", no. October, 2023, doi:  
284 10.26168/ajce.41.1.29.

285 M. Amal, B. Ramdane, and K. Mohamed, "Characterization and estimation of the swelling of  
286 Algerian clays, case of the clays of Médéa," vol. 004, 2014.

287 M. Translated, S. Ria, and N. Panjaitan, "The effect of lime content on bearing capacity and  
288 swelling potential of an expansive soil Introduction," 2014.

289 M. Ahmad *et al.* , "Predicting California bearing ratio of HARHA - treated expansive soils  
290 using Gaussian process regression," *Sci. Rep. ,* pp. 1–11, 2023, doi:10.1038/s41598-023-  
291 40903-1.

292 S. Kumar, A. Kumar, and S. Naval, "Influence of Jute Fiber on CBR Value of Expansive Soil,"  
293 vol. 6, no. 6, pp. 1180–1194, 2020.

294 HAM Abdelkader, ASA Ahmed, MMA Hussein, H. Ye, and J. Zhang, "An Experimental Study  
295 on Geotechnical Properties and Micro-Structure of Expansive Soil Stabilized with Waste  
296 Granite Dust," *Sustain. ,* flight. 14, no. 10, 2022, doi: 10.3390/su14106218.

297 **NF EN ISO 17892-1** : "Soil testing – Part 1: Determination of water content", 2016  
298 "NF P 94-051 Liquid Limit(1993).pdf."

299 A. Descriptors, "NF P 94-068 Soils: Recognition and tests Measurement of the methylene  
300 blue adsorption capacity of a soil or rock material Roads Earthworks —," pp. 1–8, 1998.

301 NF En, "Tests to determine the mechanical and physical characteristics of aggregates Part

302 6: Determination of the actual density", 2001.  
303 **NF P 94-055** : "Determination of organic matter content in soils", 1995  
304 **NF P 94-093** : "Modified Proctor test – Determination of the density and water content of  
305 soils ", 2015  
306 **NF P 94-078** : "CBR (California Bearing Ratio) test after immersion", 2015  
307 "SIZED ROAD BODY", pp. 42–52.  
308 RGDE Justification and DESSDE Chaussees, "DES COSCHES DE CHAUSSEE EN PLACE  
309 ROUTE MISSESSINTO – ALLADA SECTION MISSESSINTO - GLO".  
310 S. Des and A. Meteorologiques, "Directorate of Climatology and Applications," pp. 1–10,  
311 2023  
312

UNDER PEER REVIEW IN IJAR